The Electrostatic Driving Force for Nucleophilic Catalysis in L-Arginine Deiminase: A Combined Experimental and Theoretical Study†

Ling Li, Zhimin Li, Canhui Wang, Dingguo Xu, Patrick S. Mariano, Hua Guo,* and Debra Dunaway-Mariano*

Department of Chemistry and Chemical Biology, University of New Mexico, Albuquerque, New Mexico 87131

Received November 28, 2007; Revised Manuscript Received February 14, 2008

ABSTRACT: L-Arginine deiminase (ADI) catalyzes the hydrolysis of L-arginine to form L-citrulline and ammonia via two partial reactions. A working model of the ADI catalytic mechanism assumes nucleophilic catalysis by a stringently conserved active site Cys and general acid−general base catalysis by a stringently conserved active site His. Accordingly, in the first partial reaction, the Cys attacks the substrate guanidino C_ζ atom to form a tetrahedral covalent adduct, which is protonated by the His at the departing ammonia group to facilitate the formation of the Cys-*S*-alkylthiouronium intermediate. In the second partial reaction, the His activates a water molecule for nucleophilic addition at the thiouronium C_ζ atom to form the second tetrahedral intermediate, which eliminates the Cys in formation of the L-citrulline product. The absence of a basic residue near the Cys thiol suggested that the electrostatic environment of the Cys thiol, in the enzyme–substrate complex, stabilizes the Cys thiolate anion. The studies described in this paper explore the mechanism of stabilization of the Cys thiolate. First, the log(k_{cat}/K_m) and log k_{cat} pH rate profiles were measured for several structurally divergent ADIs to establish the pH range for ADI catalysis. All ADIs were optimally active at pH 5, which suggested that the Cys pK_a is strongly perturbed by the prevailing electrostatics of the ADI active site. The pK_a of the *Bacillus cereus* ADI (BcADI) was determined by UV−pH titration to be 9.6. In contrast, the pK_a determined by iodoacetamide Cys alkylation is 6.9. These results suggest that the negative electrostatic field from the two opposing Asp carboxylates perturbs the Cys pK_a upward in the apoenzyme and that the binding of the iodoacetamide (a truncated analogue of the citrulline product) between the Cys thiol and the two Asp carboxylates shields the Cys thiol, thereby reducing its pK_a. It is hypothesized that the bound positively charged guanidinium group of the L-arginine substrate further stabilizes the Cys thiolate. The so-called "substrate-assisted" Cys ionization, first reported by Fast and co-workers to operate in the related enzyme dimethylarginine dimethylaminohydrolase [Stone, E. M., Costello, A. L., Tierney, D. L., and Fast, W. (2006) *Biochemistry 45*, 5618–5630], was further explored computationally in ADI by using an ab initio quantum mechanics/molecular mechanics method. The energy profiles for formation of the tetrahedral intermediate in the first partial reaction were calculated for three different reaction scenarios. From these results, we conclude that catalytic turnover commences from the active configuration of the ADI(L-arginine) complex which consists of the Cys thiolate (nucleophile) and His imidazolium ion (general acid) and that the energy barriers for the nucleophilic addition of Cys thiolate to the thiouronium C_ζ atom and His imidazolium ion-assisted elimination from the tetrahedral intermediate are small.

L-Arginine deiminase (ADI)[1] catalyzes the hydrolysis of L-arginine to form citrulline and ammonia (*1, 2*) (Scheme 1). This reaction is the first step in the L-arginine dihydrolase pathway (*3, 4*), which allows specialized bacterial pathogens to use L-arginine as a source of ammonia and ATP (*5–9*). The ADI gene has also been found in the primitive eukaryote *Giardia lamblia* (*10*), a highly contagious protozoan parasite that causes giardiasis in humans (*11*). Because of its potential threat to water and food supplies, *G. lamblia* is classified as a biodefense category B pathogen. Aside from energy production in the *G. lamblia* trophozoite residing in the lumen of the small intestine, the arginine dihydrolase pathway serves to supply the ammonia required for the

† This work is supported by NIH Grant AI-059733 to D.D.-M. and P.S.M. and by NIH Grant R03AI068672 to H.G.

* To whom correspondence should be addressed. Experimental work: Debra Dunaway-Mariano, Department of Chemistry and Chemical Biology, University of New Mexico, Albuquerque, NM 87131; e-mail, dd39@unm.edu; fax, (505) 277-6206; telephone, (505) 277-3383. Theoretical work: Hua Guo, Department of Chemistry and Chemical Biology, University of New Mexico, Albuquerque, NM 87131; e-mail, hguo@unm.edu; fax, (505) 277-2609; telephone, (505) 277-1716.

[1] Abbreviations: ADI, arginine deiminase; PaADI, *Pseudomonas aeruginosa* ADI; BcADI, *Bacillus cereus* ADI; EcADI, *Escherichia coli* ADI; BmADI, *Burkholderia mallei* ADI; DDAH, dimethylarginine dimethylaminohydrolase; PAD, peptidyl-arginine deiminase; ADMA, N^G,N^G-dimethyl-L-arginine; DFT, density functional theory; GMSF, guanidino group-modifying enzyme superfamily; MD, molecular dynamics; QM/MM, quantum mechanical/molecular mechanical; IPTG, isopropyl β-D-thiogalactopyranoside; DTT, dithiothreitol; NADH, reduced form of nicotinamide adenine dinucleotide; MES, 2-(*N*-morpholino)ethanesulfonic acid; Bis-Tris, [bis(2-hydroxyethyl)amino]-tris(hydroxymethyl)methane; HEPES, *N*-(2-hydroxyethyl)piperazine-*N*′-2-ethanesulfonic acid; Tris, tris(hydroxymethyl)aminomethane; TAPS, 3-{[tris(hydroxymethyl)methyl]amino}propanesulfonic acid; CHES, 2-(*N*-cyclohexylamino)ethanesulfonic acid; CAPS, 3-(cyclohexylamino)propanesulfonic acid.

10.1021/bi7023496 CCC: $40.75
Published on Web 03/27/2008

Scheme 1

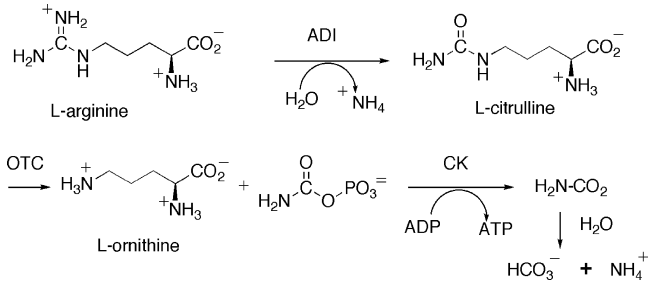

synthesis of glucoseamine-6-phosphate for cyst wall polysaccharide biosynthesis (*12*). Furthermore, the impact of the *G. lamblia* trophozoite on the L-arginine pool available to the human nitric oxide synthase may result in a weakened host defense system (*13, 14*). The arginine dihydrolase pathway, which is not present in humans, represents an attractive target for the development of antibacterial and antiparasitic drugs.

ADI is a member of the hydrolytic branch of the guanidino group-modifying enzyme superfamily (GMSF) (*15*). Other branch members include dimethylarginine dimethylaminohydrolase (DDAH) which catalyzes the hydrolysis of N^G,N^G-dimethyl-L-arginine (ADMA) to form dimethylamine and citrulline (*16, 17*); peptidyl-arginine deiminase (PAD) (*18*), which catalyzes the deimination of the guanidino group from carboxyl-terminal arginine residues of peptides; agmatine deiminase, which catalyzes the hydrolysis of agmatine to form ammonia and *N*-carbamoylputrescine (*19*); and *N*-succinylarginine dihydrolase, which catalyzes the transfer of an amidino group from *N*-succinylarginine followed by hydrolytic deimination to form ornithine and ammonia (*20*). Through ADMA, DDAH is known to control the level of NO produced by nitric oxide synthase (*21*), the dysregulation of which is related to an array of diseases such as hypertension and diabetes. The human PADs (e.g., PAD4) are involved in post-translational histone modification (*22, 23*), and they are associated with many debilitating human diseases, including rheumatoid arthritis (*24*). An improved understanding of the catalytic mechanisms of these enzymes will inevitably aid in the design of new therapeutic agents.

To date, more than 20 structures have been determined for members of the GMSF (*20, 25–34*). These structures show that the overall fold and catalytic scaffold of these enzymes are similar, despite a considerable degree of sequence diversity (*15*). The key catalytic residues are the Cys, which functions in nucleophilic catalysis, and the His, which functions in general acid−general base catalysis (*20, 26, 30, 32, 33, 35, 36*). As shown in Figure 1, the proposed mechanism involves nucleophilic attack of the substrate guanidino C_ζ atom by the Cys thiolate, yielding a tetrahedral covalent adduct. His-assisted expulsion of ammonia leads to the *S*-alkylthiouronium intermediate, which is then hydrolyzed by the His-activated water nucleophile. The GMSF active sites are spatially restricted, highly electrostatic, and gated by substrate-induced loop closure. There is minimal overlap in substrate activities between GMSF enzymes (*22, 32, 36, 37*). So far, strategies for inhibitor design have targeted the Cys nucleophile for covalent modification (*33, 38–41*).

Studies in our laboratories have focused on the mechanisms of substrate recognition and catalysis in *Pseudomonas aeruginosa* ADI (PaADI). In addition to the Cys406 and His278 catalytic residues of PaADI, the active site contains numerous polar substrate-binding residues. The guanidino group of the arginine substrate is held in place by hydrogen bonds with the carboxylate groups of Asp280 and Asp166, while the carboxyl and amino groups are also engaged in hydrogen bonds with polar residues (Arg243, Arg185, and Asn160 side chains; Leu41 C═O group) located near the active site entrance (Figure 2) (*26, 30*). The removal of any one of the substrate−enzyme interactions has been shown to severely impair catalytic function (*2, 37, 42*), and the strengths of active site hydrogen bonds have been confirmed by molecular dynamics (MD) studies (*43*). These observations point to the importance of electrostatic interactions in ADI catalysis.

Inspection of the PaADI active site structure (*29, 30*) reveals that the Cys nucleophile is not juxtaposed with a basic residue, which might activate it by deprotonation. Therefore, ADI must employ electrostatic forces to stabilize the Cys thiolate so that it is present at the pH required for catalytic function, which for PaADI is acidic (pH 5) (*37*). What constitutes the electrostatic interactions in the PaADI active site that serve this function? The X-ray structures of the apo and substrate-bound PaADI show that the His278 imidazole ring is anchored by the Glu224 carboxylate (*29, 30*). At a distance of 7 Å, the imidazolium unit of the protonated His278 is too distant to engage in a strong electrostatic interaction with the Cys406 thiol.

In this study, we have measured the pH rate profiles for several ADIs from divergent organisms to define the limits of the pH range within which the His-Cys catalytic pair can operate. Next, we measured the pK_a of the Cys thiol in apo ADI and in the liganded ADI. Finally, we carried out QM/MM calculations, using the coordinates from the published ADI X-ray structures (*29, 30*), to define the ionization states of the Cys and His residues and their impact on the reaction. The results presented below suggest that the Cys thiol ionization in the apoenzyme is suppressed because of unfavorable charge–charge interactions with the two Asp neighbors. The bound substrate L-arginine creates a shield for the charge–charge repulsion between the Cys thiolate and the Asp carboxylates and provides the Cys thiolate anion with a cation for ion pair formation. When substrate binds, the Cys thiol loses its proton to solvent. Catalytic turnover commences from the active configuration of the ADI(L-arginine) complex [which consists of the Cys thiolate (nucleophile) and His imidazolium ion (general acid)] and proceeds through two low-energy barriers to the tetrahedral intermediate of partial reaction 1 (Figure 1).

MATERIALS AND METHODS

Preparation of ADIs. Recombinant PaADI was prepared as described in ref *37*. The genes encoding *Bacillus cereus* ADI (BcADI) (*44*), *Escherichia coli* ADI (EcADI), and *Burkholderia mallei* ADI (BmADI) were cloned using a PCR-based strategy with *Pfu* DNA polymerase (Stratagene), genomic DNA (Bc ATCC 10987D; Ec ATCC 700928D; Bm ATCC 23344), and commercial primers. The PCR product was purified by gel electrophoresis, digested with NdeI and BamHI (Invitrogen), and ligated into the pET-3c expression vector (Novagen). The clone, NdeI-BamHI-pET3c-ADI, was used to transform competent *E. coli* BL21(DE3) cells. Gene

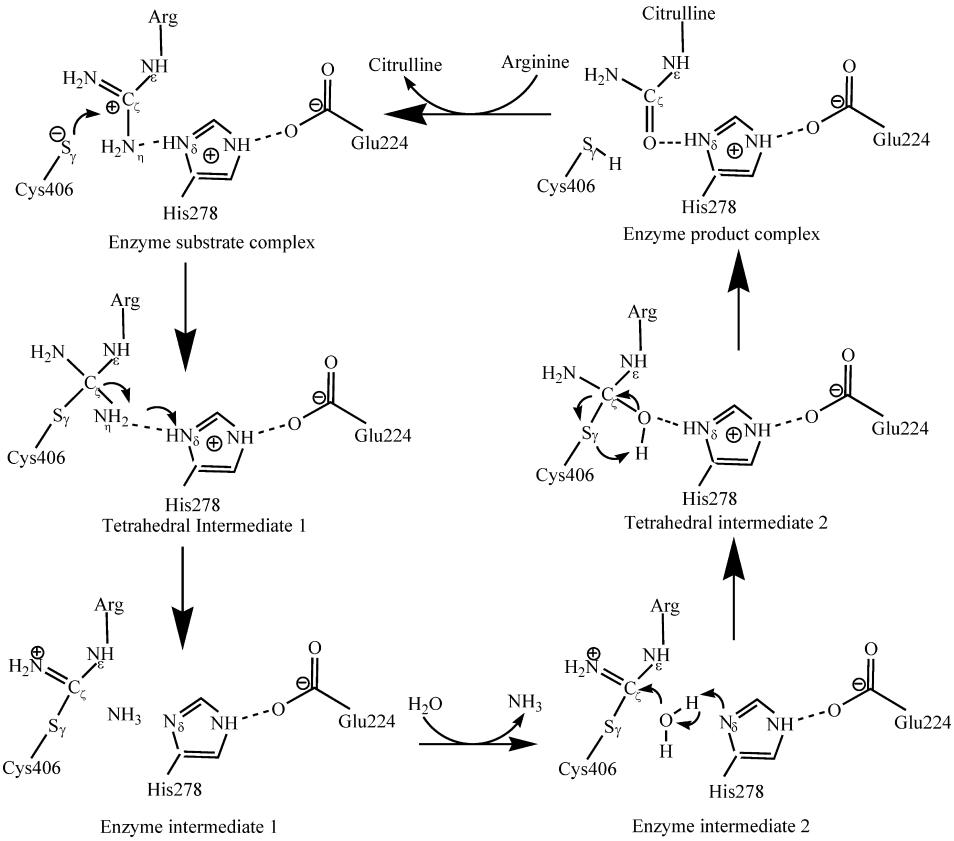

FIGURE 1: Proposed steps of the hydrolytic deimination of L-arginine catalyzed by arginine deiminase.

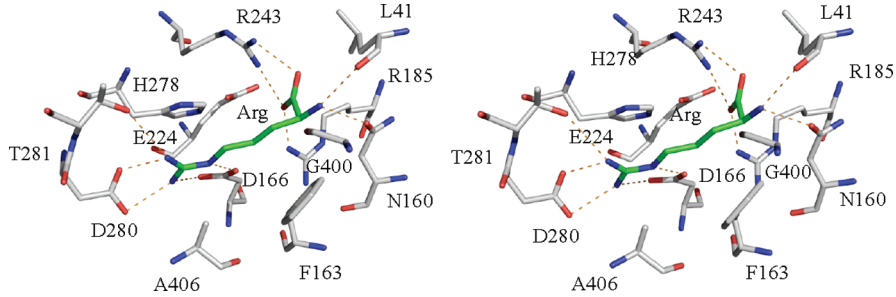

FIGURE 2: Stereodiagram representation of the PaADI C406A active site bound with L-arginine (*30*). This figure was prepared using the graphics program PyMol and the X-ray crystallographic coordinates of entry 2A9G in the Protein Data Bank. Oxygen atoms are colored red, nitrogen atoms blue, and carbon atoms gray (enzyme) or green (L-arginine).

sequences were verified by DNA sequencing (Center for Genetics in Medicine, University of New Mexico School of Medicine, Albuquerque, NM). Transformed *E. coli* BL21(DE3) cells were grown in Luria broth (LB) containing 50 μg/mL ampicillin, with mixing at 180 rpm and 20 °C (EcADI and BmADI) or 25 °C (BcADI). The cells were induced with 0.4 mM isopropyl β-D-thiogalactopyranoside (IPTG) once the OD_{600} of the culture reached 0.6–0.8. After 4 h, the cells were harvested by centrifugation (6500 rpm, 15 min, 4 °C). The cell pellet (30 g) was suspended in 300 mL of ice-cold buffer A [50 mM K^+HEPES containing 1 mM dithiothreitol (DTT) (pH 7.5)] and the mixture passed through a French press at 1200 psi. The supernatant obtained by centrifugation (20000 rpm, 30 min, 4 °C) of the cell lysate was collected and subjected to column chromatography. The supernatant was loaded directly onto a 40 cm × 5 cm DEAE-cellulose (EcADI and BmADI) or 40 cm × 5 cm (BcADI) DEAE-Sepharose column at 4 °C, and then the column was eluted with 1 L of buffer A followed by a 2 L linear gradient from 0 to 0.4 M KCl in buffer A. The EcADI and the BmADI-containing fractions were separately combined, mixed with ammonium sulfate (10%, grams per milliliter), and loaded onto 18 cm × 3 cm Butyl-Sepharose columns (Sigma) pre-equilibrated with buffer A containing 10% (grams per milliliter) ammonium sulfate. The columns were eluted at 4 °C with 300 mL of buffer A containing 10% (grams per milliliter) ammonium sulfate followed by a 800 mL linear gradient from 10% (grams per milliliter) to 0% ammonium sulfate in buffer A. Following concentration and dialysis, the purified EcADI and BmADI were shown by SDS−PAGE analysis (Figure SI1A of the Supporting Information) to be homogeneous. The yield was ca. 2 mg of protein/g of wet cells. The 280 nm molar extinction coefficients are 37500 and 41560 M^{-1} cm^{-1} for EcADI and BmADI, respectively. The theoretical mass of EcADI is 45902 Da, and the experimental mass determined by ES mass spectrometry is 45901 Da. The theoretical mass of BmADI is 46052 Da, and the experimental mass determined by ES mass spectrometry is 45921 Da, which indicates that the BmADI

N-terminal Met residue is removed by post-translational modification.

The BcADI-containing DEAE column fractions were combined, dialyzed against 3 × 2 L of buffer A, and then loaded onto a 27 cm × 3 cm hydroxyapatite fast flow column (Sigma), pre-equilibrated with buffer A. The column was eluted at 4 °C with 300 mL of buffer A followed by a 600 mL linear gradient from 0 to 0.4 M KH_2PO_4 in buffer A. Fractions containing BcADI were combined, dialyzed against 3 × 2 L of buffer A, and then loaded onto a 27 cm × 3 cm hydroxyapatite high-resolution column (Sigma), pre-equilibrated with buffer A. The column was eluted at 4 °C with 300 mL of buffer A followed by a 600 mL linear gradient from 0 to 0.4 M KH_2PO_4 in buffer A. Following concentration and dialysis, the purified BcADI was shown by SDS−PAGE analysis (Figure SI1B of the Supporting Information) to be homogeneous. The yield was ca. 10 mg of protein/g of wet cells. The 280 nm BcADI molar extinction coefficient is 32650 M^{-1} cm^{-1}. The theoretical mass of BcADI is 46938 Da, and the experimental mass determined by ES mass spectrometry is 46938 Da.

Preparation of BcADI Mutants. The BcADI C400S, C265S, C265S/C336S, and C265S/C336S/C400S mutant genes were generated by using the polymerase chain reaction with plasmid NdeI-BamHI-pET3c-ADI containing the BcADI gene as a template, and commercial oligonucleotides as primers. The PCR products were digested with NdeI and BamHI restriction enzymes. The DNA fragments were purified by agarose gel chromatography and then ligated into the NdeI-BamHI-pET3c-ADI vector plasmid (digested with the same restriction enzymes) using T4 DNA ligase. The resulting clones were transformed into competent *E. coli* BL21(DE3) cells for gene expression. The sequence of each mutant was verified by DNA sequencing (Center for Genetics in Medicine, University of New Mexico School of Medicine). The C265S and C400S mutant genes were constructed by using the wild-type gene as a template. The BcADI C265S/C336S gene was constructed by using the BcADI C265S gene as a template, and the BcADI C265S/C336S/C400S gene was constructed using the BcADI C265S/C336S gene as a template. The BcADI mutant proteins were purified using the same procedure used to purify the wild-type enzyme (*vide infra*). The homogeneity of each mutant enzyme was confirmed by SDS−PAGE analysis. The turnover rate of the wild-type BcADI measured at pH 7.5 and 25 °C by using the continuous kinetic assay described below is 4 s^{-1}. The turnover rates of the BcADI mutants are as follows: 6 s^{-1} for C265S, 1 s^{-1} for C336S, 1 s^{-1} for C265S/C336S, $<1 \times 10^{-4}$ s^{-1} for C400S, and $<1 \times 10^{-4}$ s^{-1} for C265S/C336S/C400S.

ADI Activity Assays and Determination of Steady-State Kinetic Constants. The fixed-time colorimetric assay for determination of citrulline generated by ADI-catalyzed L-arginine hydrolysis is based on the procedure reported in ref *45*. Accordingly, for the assessment of citrulline, at a specific time point, an aliquot (250 μL) of the reaction solution was withdrawn and mixed with 1 mL of a mixture of one part of oxime reagent (0.8 g of 2,3-butanedione 2-oxime in 100 mL of 5% acetic acid) and two parts of antipyrine/sulfuric acid reagent (5 g of antipyrine in 1000 mL of 50% sulfuric acid). The mixture was placed in a 60 °C water bath for 80 min, and the absorbance at 466 nm was measured immediately.

The continuous spectrophotometric assay for the assessment of ammonia generated by ADI-catalyzed L-arginine hydrolysis is based on the procedure reported in ref *46*. Reaction solutions containing L-arginine and ADI also initially include 1.8 mg/mL glutamate dehydrogenase (bovine liver, type II), 10 mM ketoglutarate, and 0.2 mM NADH in 50 mM K^+HEPES at pH 7.0. The progress of the reaction is monitored by measuring the decrease in solution absorption at 340 nm ($\Delta\epsilon = 6.22$ mM^{-1} cm^{-1}).

The k_{cat} and K_m values were determined from the initial velocity of the ADI-catalyzed reaction measured as a function of substrate concentration. The initial velocity data were fitted to eq 1 using KinetAsyst.

$$V = V_{max}[S]/([S] + K_m) \quad (1)$$

where V is the initial velocity, V_{max} is the maximum velocity, [S] is the substrate concentration, and K_m is the Michaelis constant. The k_{cat} value was calculated from the V_{max} and enzyme concentration ([E]) according to the equation $k_{cat} = V_{max}/[E]$.

ADI pH Rate Profile Determination. For pH rate profile determinations, the following buffers were used: 25 mM MES and 25 mM acetate for pH 5.0, 50 mM MES for pH 5.6, 50 mM Bis-Tris for pH 6.0 and 6.5, 50 mM HEPES for pH 7.0 and 7.5, 50 mM Tris for pH 8.0, 50 mM TAPS for pH 8.5, CHES for pH 9–9.5, and CAPS for pH 10–10.5. Initial velocities of ADI-catalyzed L-arginine hydrolysis were measured at different solution pH values, as a function of substrate concentration (0.5–10 × K_m), by using the fixed-time colorimetric ADI activity assay described above. The stability of ADI in the reaction solution was checked by preincubation of the enzyme in the reaction solution buffer followed by activity determination at the optimal pH. In addition, buffer inhibition was checked by comparing reaction rates for buffer pairs measured at the same pH. The k_{cat} and k_{cat}/K_m values calculated from the initial velocity data were fitted to eq 2 for the ionization of an essential acid or to eq 4 for the ionization of an essential acid and the ionization of the protonated form of an essential base.

$$\log Y = \log[C/(1 + H/K_a)] \quad (2)$$

$$\log Y = \log[C/(1 + H/K_a + K_b/H)] \quad (3)$$

where Y is the k_{cat} or k_{cat}/K_m, H is the proton concentration of the reaction solution, K_a and K_b are the apparent ionization constants of the acidic and basic groups, respectively, and C is the constant value of Y where it does not change with the solution pH.

Determination of the BcADI Cys pK_a by UV-Monitored pH Titration. UV difference spectra (200–400 nm) were measured for buffered solutions containing 37 μM wild-type BcADI and C400S BcADI as a function of pH, within the pH range of 4−10.5. UV difference spectra were also measured for buffered solutions of 30 μM C265S/C336S BcADI and C265S/C336S/C400S BcADI as a function of pH, within the pH range of 7−10. The following buffers (50 mM) and pH values were used: MES and potassium acetate at pH 4.0–5.0, MES at pH 5.5, Bis-Tris at pH 6–6.5, HEPES at pH 7–8, TAPS at pH 8.5, CHES at pH 9–9.5, and CAPS at pH 10–10.5. The absorbance difference at 244

nm versus pH data were fitted to eq 4 with Kaleidagraph to define the acid dissociation constant K_a.

$$A = (A_L[H] + A_H K_a)/(K_a + [H]) \quad (4)$$

where A is the absorbance difference, [H] is the proton concentration of the reaction solution, and A_L and A_H are the minimum and maximum values of absorbance difference, respectively.

Inactivation of C265S/C336S BcADI with Iodoacetamide. Inactivation reactions were carried out by adding iodoacetamide (final concentrations of 1–20 mM) to 30 μM C265S/C336S BcADI in 50 mM MES (pH 5.5) on ice. After specified time periods, 10 μL aliquots were removed and assayed by using the continuous assay for ADI-catalyzed hydrolysis of L-arginine. The assay mixtures contained 4 mM DTT, which is at ca. 10–200-fold molar excess over iodoacetamide, to quench the alkylation reaction. The maximum concentration of iodoacetamide transferred to the assay mixture is 20 μM, which independent tests showed is not inhibitory toward glutamate dehydrogenase. Natural logs of the ratios of v_t for the enzyme incubated with iodoacetamide at a specified time (t) to the v_0 of the enzyme incubated in buffer without iodoacetamide were plotted against time. The observed pseudo-first-order rate constants for the inactivation (k_{obs}) were derived from the slopes of these plots as defined by eq 5. The resulting k_{obs} values were plotted against iodoacetamide concentration. The data were fitted by using Kaleidagraph to eq 6 to obtain the values of K_I (concentration of iodoacetamide that corresponds to 50% inactivation) and k_{inact} (the inactivation rate constant).

$$\ln(v_t/v_0) = k_{obs}t \quad (5)$$

$$k_{obs} = (k_{inact}[I])/(K_I + [I]) \quad (6)$$

pH Dependence of the Rates of Iodoacetamide Inactivation of the C265S/C336S BcADI Mutant. The C265S/C336S BcADI mutant (80 μM) was incubated at 25 °C with 1.5 mM iodoacetamide in the following buffers (50 mM): MES and potassium acetate at pH 4.0–5.0, MES at pH 5.5, Bis-Tris at pH 6–6.5, HEPES at pH 7–8, Taps at pH 8.5, CHES at pH 9–9.5, and CAPS at pH 10–10.5. Aliquots (5 μL) were removed at various times and assayed by using the continuous assay for ADI-catalyzed arginine hydrolysis. The pH profile data [log(k_{obs}) vs pH] were fitted to eq 7 with Kaleidagraph.

$$\log Y = \log[Y_L + Y_H(K/[H])/(1 + K/[H])] \quad (7)$$

where K is the acid dissociation constant, Y is the k_{obs} at the hydrogen ion concentration [H], and Y_L and Y_H are the minimum and maximum values of k_{obs}, respectively.

Theoretical Models. For the QM/MM calculations, all the heavy atom coordinates were adopted from the crystal structure (PDB entry 2A9G) of the C406A mutant ADI from *P. aeruginosa* complexed with the L-arginine substrate (*30*). The wild-type enzyme was recovered via replacement of the Ala406 side chain with that of Cys. The Cys rotomer that places the sulfur atom closest to the substrate guanidino carbon was chosen. Hydrogen atoms were then added by the HBUILD module of CHARMM (*47*). The enzyme–substrate (ES) complexes were solvated repeatedly with a pre-equilibrated TIP3P water sphere centered at the guanidino carbon atom with a radius of 25 Å. Any solvent water molecule that came within a 2.8 Å radius of a non-hydrogen atom in the protein was deleted. This was followed by relaxation of the solvent water sphere with all protein atoms and crystal waters fixed. Using the stochastic boundary protocol (*48*), the solvated system was divided into the reaction region (r < 22 Å) and buffer region (22 Å < r < 25 Å), with atoms outside the 25 Å radius deleted. The innermost reaction zone (r < 22 Å) is governed by the potential generated by the hybrid QM/MM scheme (*vide infra*). The atoms in the buffer zone are also subjected to harmonic constraints and solvent boundary potentials such that the system remains close to the experimental structure. The energy of the entire system was then minimized using both the conjugated gradient method and the adoptive basis Newton–Raphson method.

The QM/MM approach (*49, 50*) was used to include a large portion of the solvated enzyme in the simulation of the bond breaking and forming processes. Because of the involvement of sulfur in the reaction, the commonly used AM1 and PM3 semiempirical methods are not suitable (*51*), and instead, the approach is based on a B3LYP (Becke3−Lee–Yang–Parr) (*52, 53*) treatment of the QM region, coupled with the CHARMM22 all atom force field (*54*) for the MM region. The choice of DFT is influenced by its (partial) inclusion of the electronic correlation, which is important in accurately describing the barrier and exothermicity for chemical reactions. In our systems, the QM region includes side chains of Cys406, His278, and Glu224 and the substrate ligand. All atoms in the system except sulfur were treated with the standard 6-31G** basis set. Because of the anionic nature of the thiolate moiety, diffuse functions were added in the sulfur atom basis set (6-31+G**). At the QM/MM boundary, the link atom approach was used to saturate the dangling bonds (*55*). Specifically, link atoms were added between C_α and C_β atoms of Cys406 and His278, between C_β and C_γ atoms of Glu224, and between C_γ and C_δ atoms of the arginine substrate. For models I, II, and III, there are 38, 37, and 38 QM atoms, respectively, while the total number of atoms is around 7600. The reaction path was determined by adiabatic mapping, in which the entire QM/MM system is relaxed at fixed values of the reaction coordinate. For this purpose, the CHARMM−GAMESS interface was used (*49*) and the convergence criterion was set to be a gradient root-mean-square deviation of <0.05 kcal mol^{-1} Å^{-1}.

RESULTS AND DISCUSSION

ADI pH Rate Profiles. The pH rate profiles for ADI catalysis of L-arginine hydrolysis were measured using the fixed-time colorimetric assay for citrulline. The pH rate profile measured for the ADI from *P. aeruginosa* (PaADI) in a previous study (*37*) showed that efficient catalytic turnover takes place in an acidic solution (pH 5–5.6). Under these conditions, the catalytic His278 functions as a general acid in the first partial reaction and as a general base in the second partial reaction (Figure 1). The catalytic Cys406 must be ionized to function as a nucleophile in the first partial reaction.

The catalytic efficiency of PaADI within its optimal pH range is modest (measured at pH 5.6 and 25 °C, k_{cat} = 6 s^{-1}, K_m = 140 μM, and k_{cat}/K_m = 5 × 10^4 s^{-1} M^{-1}) and is

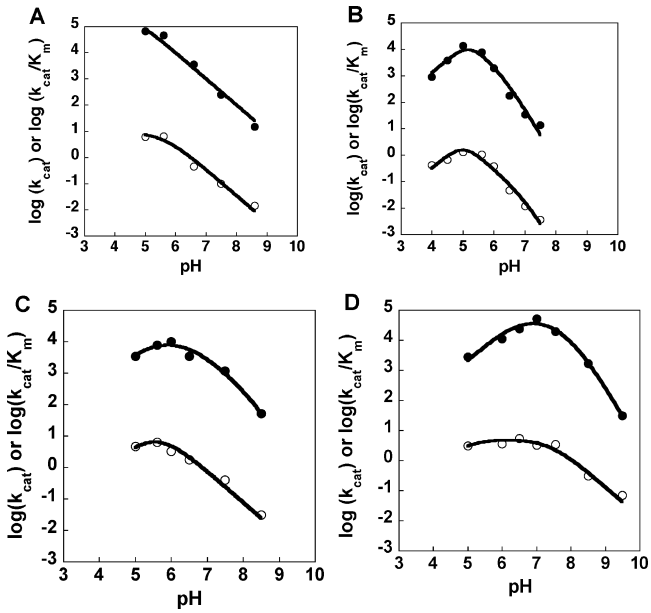

FIGURE 3: pH rate profiles of ADI-catalyzed hydrolysis of L-arginine to citrulline and ammonia: (○) log k_{cat} vs pH and (●) log(k_{cat}/K_m) vs pH. See Materials and Methods for details. (A) For PaADI, from k_{cat} data and eq 3 pK_a = 5.6 ± 0.3 and from k_{cat}/K_m data and eq 2 pK_a = 4 ± 1. (B) For BmADI, from k_{cat} data and eq 3 pK_a = 5 ± 1 and from k_{cat}/K_m data and eq 3 pK_a = 6.5 ± 0.6. (C) For EcADI, from k_{cat} data and eq 3 pK_a = 5.2 ± 0.2 and from k_{cat}/K_m data and eq 3 pK_a = 5.3 ± 0.5. (D) For BcADI, from k_{cat} data and eq 2 pK_a = 7.6 ± 0.2 and from k_{cat}/K_m data and eq 3 pK_a = 7.4 ± 0.6.

Table 1: Kinetic Rate Constants for ADI-Catalyzed Conversion of L-Arginine to L-Citrulline and Ammonia[a]

ADI	pH	k_{cat} (s^{-1})	K_M (mM)	k_{cat}/K_M (M^{-1} s^{-1})
PaADI[b,c]	5.6	6.3 ± 0.1	0.14 ± 0.01	4.5×10^4
BmADI[c]	5.6	1.3 ± 0.1	0.09 ± 0.01	1.4×10^4
EcADI[c]	6.0	3.2 ± 0.1	0.32 ± 0.02	1.0×10^4
BcADI[c]	7.0	3.2 ± 0.2	0.06 ± 0.01	5.1×10^4
BcADI[d]	7.0	4.4 ± 0.1	0.09 ± 0.01	4.9×10^4

[a] See Materials and Methods for details. [b] Kinetic constants, measured using the fixed-time colorimetric assay which monitors citrulline formation, are taken from ref (*37*). [c] Kinetic constants were determined using the fixed-time colorimetric assay which monitors citrulline formation. [d] Kinetic constants were determined using the continuous coupled assay which monitors ammonia formation.

significantly lower than that of ADI from *Mycoplasma arthritidis* which was measured at pH 7.2 and 25 °C (k_{cat} = 29 s^{-1}, K_m = 4 μM, and k_{cat}/K_m = 7 × 10^6 s^{-1} M^{-1}) (*2*). Although the pH rate profile of the *M. arthritidis* ADI to our knowledge has not been reported, the enzyme has been reported to function efficiently at neutral pH. The change in the kinetic behavior that accompanies the sequence divergence (82% sequence nonidentity) of PaADI and *M. arthritidis* ADI suggested that to understand the electrostatic forces that contribute to ADI catalysis, it would be advantageous to examine the kinetic behavior of ADIs derived from a variety of biological systems.

For this reason, we have measured pH rate profiles for the ADIs from *B. cereus* (BcADI), *E. coli* (EcADI), and *B. mallei* (BmADI) (Figure 3). BmADI, which is a close sequence homologue of PaADI (78% identical), shares with PaADI the pH 5 optimum for k_{cat} and the modest level of catalytic efficiency (Table 1). The sequence of EcADI is 45% identical with those of PaADI and BmADI. It too functions maximally at pH 5 and does so with modest catalytic efficiency. The sequence of BcADI is only ~35% pairwise identical with PaADI, BmADI, and EcADI. BcADI is optimally active at acidic and at slightly alkaline pH (4.4–7.8), yet it is significantly less efficient than *M. arthritidis* ADI, with which it shares 36% sequence identity. Because of the fact that BcADI is active at neutral pH, we were able to use the same ammonia-based assay employed to measure the activity of *M. arthritidis* ADI. The kinetic constants agree closely with the kinetic constants obtained with the citrulline-based assay (Table 1). Thus, the difference between the catalytic efficiencies of PaADI, BmADI, EcADI, and BcADI versus *M. arthritidis* ADI cannot be attributed to differences in the activity assays used.

We conclude that all ADIs sampled perform well in acidic solution (as low as pH 5). The liganded structures of the PaADI (*30*) and the *M. arthritidis* ADI (*26*) do not provide obvious clues about the observed difference in their kinetic behavior at neutral pH.

Difference UV Spectroscopy for Cys-Thiol pK_a Determination. The ionization of a solvated Cys thiol to form the corresponding thiolate anion is accompanied by an increase in absorption within the 230−250 nm wavelength range (*57*). This property has been previously exploited to determine the pK_a values of protein Cys residues (*58–63*). For these determinations, the difference in absorbance (typically at 240 nm) between the wild-type enzyme and the Cys-to-Ser mutant is monitored as a function of solution pH. The absorption changes are used to measure the concentration of the Cys thiolate (assuming that the Cys-to-Ser mutation does not indirectly alter the 240 nm absorption).

Of the four ADIs that were studied, BcADI is the most robust over a wide pH range and thus was selected for the nucleophilic Cys pK_a determination. BcADI contains two nonconserved Cys residues, Cys265 and Cys336 (both located at the protein surface), in addition to the invariant catalytic Cys400. By measuring the difference spectrum between wild-type BcADI and the C400S ADI mutant as a function of solution pH and plotting the absorbance at 244 nm as a function of solution pH (Figure 4A), we obtained the titration profile shown in Figure 4B. Data fitting to eq 4 (see Materials and Methods) defined a pK_a value of 9.6 ± 0.1. The observed ε at 244 nm is 10 mM^{-1} cm^{-1} which compares with the reported thiolate ε value of 5.2 mM^{-1} cm^{-1} (*57*).

To assign unequivocally the UV−pH titration response of BcADI to Cys400, the double mutant C265S/C336S BcADI was prepared and subjected to the titration procedure. This mutant is catalytically active (k_{cat} = 1 s^{-1} vs 4 s^{-1} for the wild-type enzyme). Analysis of the pH dependence of the UV difference spectrum between C265S/C336S and C265S/C336S/C400S was carried out in a similar manner to define the pK_a of Cys400 in the C265S/C336S mutant as 9.5 ± 0.1 (Figure 4C,D). Thus, replacement of Cys265 and Cys336 of Ser does not alter the pK_a of Cys400.

The inflection points observed in both titration curves are shifted well above the pK_a value (ca. 8.5) of free cysteine, suggesting that Cys400 has a significantly elevated pK_a in the absence of substrate bound in the active site (see refs *64* and *65* for other examples of an elevated Cys pK_a). Inspection of the ADI active site (*29, 30*) reveals a possible reason why Cys400 of the apo form of the enzyme has an unusually high pK_a. Specifically, the thiol faces the charged carboxylate

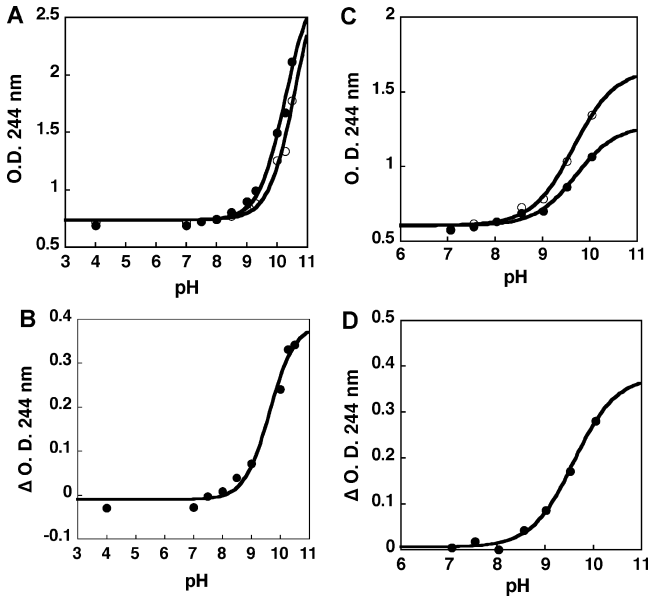

FIGURE 4: pK_a determination for the BcADI Cys400 thiol. (A) UV difference spectra of wild-type BcADI and C400S BcADI measured as a function of solution pH. (B) Plot of OD_{244} from difference spectra shown in panel A fitted to eq 4 to define the Cys400 thiol pK_a. (C) UV difference spectra of C265S/C336S BcADI and C265S/C336S/C400S BcADI measured as a function of solution pH. (D) Plot of OD_{244} from difference spectra shown in panel C fitted to eq 4 to define the Cys400 thiol pK_a.

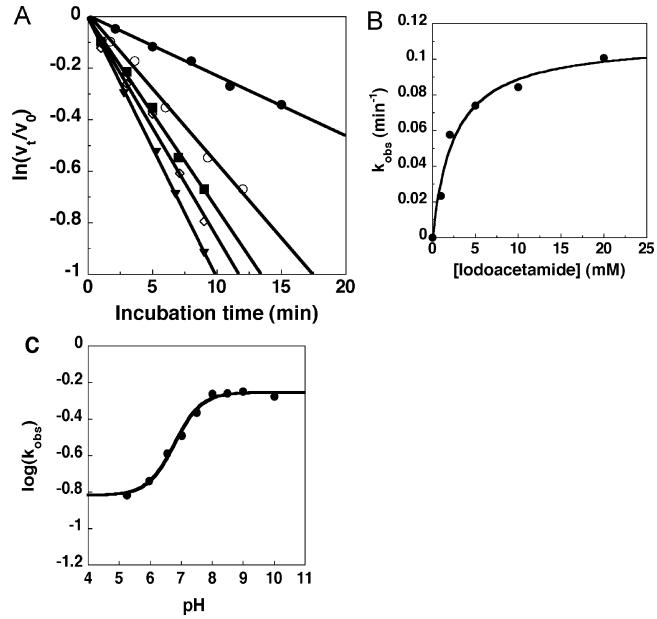

FIGURE 5: C265S/C336S BcADI inactivation by iodoacetamide on ice at pH 5.5 with 50 mM K^+MES. (A) Plots of $\ln(v_t/v_o)$ vs time for reactions of 30 μM C265S/C336S BcADI with 1 (●), 2 (○), 5 (■), 10 (◇), and 20 mM iodoacetamide (▼) on ice at pH 5.5, fitted with a linear equation (eq 5) to define k_{obs}. (B) Plot of k_{obs} vs iodoacetamide concentration fitted to eq 6 to define k_{inact} and K_I. (C) Plot of $\log(k_{obs})$ measured for the inactivation of C265S/C336S BcADI (80 μM) with 1.5 mM iodoacetamide and 25 °C vs reaction solution pH fitted to eq 7 to define the Cys400 thiol pK_a.

groups of the two catalytic Asp residues (D161 and D272) [see the PaADI active site in Figure 2 of this paper and the superimposed PaADI and BcADI active sites in Figure 13 of ref *44*]. We hypothesize that these charge–charge interactions destabilize the Cys thiolate anion.

pH Dependence of Inactivation of Wild-Type and C265S/C336S BcADI by Iodoacetamide. The pK_a of the apo BcADI active site Cys is too high to account for the optimal pH range defined by the $\log(k_{cat})$ pH profile for BcADI catalysis (Figure 3D). The question addressed here is whether the binding of substrate to the active site reduces the pK_a of the Cys thiol. Fast and co-workers have shown that the pK_a of the DDAH active site Cys thiol is reduced from 8.9 in the apoenzyme to less than or equal to pH 7.3 in the DDAH(l-lysine) complex (*62*). They attributed this decrease in pK_a to the favorable interaction of the charged ammonium side chain of the lysine ligand with the Cys thiolate anion (a citrulline ligand did not alter the Cys thiol pK_a). The bound L-dimethylarginine substrate is expected to produce the same effect observed with the lysine ligand and, thus, account for the shift in the pH optimum range of 8–9 evidenced by the $\log(k_{cat}/K_m)$ pH profile for DDAH catalysis, to within the pH optimum range of 7–8.5 as evidenced by the log k_{cat} profile (*62*).

Unfortunately, L-lysine does not bind tightly enough to ADI to allow us to test the effect of the charged ammonium side chain of the lysine ligand on the pK_a of the active site Cys thiol. Instead, an alternative method that employed the Cys thiolate alkylating agent iodoacetamide as an active site-directed irreversible inhibitor was used to test ligand-induced perturbation of the catalytic Cys thiol pK_a. Because iodoacetamide has a headgroup structurally analogous to that of the ADI product L-citrulline, it is likely that it binds between the active site Cys400 and the opposing Asp161 and Asp272 residues during the alkylation process. Although iodoacetamide does not possess the positive charge of the L-arginine substrate to stabilize the Cys thiolate anion, by binding between the thiol and the two Asp carboxylate groups it shields the Cys thiolate anion from unfavorable charge–charge interaction. Thus, if the high pK_a observed for the apo BcADI Cys400 is the result of electrostatic interaction with the conserved Asp161 and Asp272 residues, we anticipate that the iodoacetamide ligand will cause a reduction in the observed pK_a of the BcADI Cys400 thiol.

Iodoacetamide is a relatively specific alkylating agent of protein Cys residues (*66*). Because the Cys thiolate is significantly more reactive than the thiol, the rate constant for ADI alkylation by this reagent reflects the ratio of the catalytic Cys thiolate to thiol present at the prevailing solution pH. Provided that the reasonable assumption that the rate of loss of a proton from the Cys is rapid compared to the rate of thiolate alkylation holds, the k_{obs} for alkylation reflects the equilibrium concentrations of the thiol and thiolate in the presence of iodoacetamide. Thus, the pK_a value of the Cys thiol when iodoactamide is bound in the active site can be determined by measuring the pH dependence of the k_{obs} for alkylation.

Iodoacetamide alkylates all three Cys residues in BcADI (see Figure SI2 of the Supporting Information). For this reason, the catalytically active C265S/C336S BcADI mutant rather than native BcADI was used for the pK_a determination studies. The time and concentration dependence of iodoacetamide-induced inactivation of C265S/C336S BcADI, measured at pH 5.5 and 0 °C, are shown in Figure 5A. The plot of k_{obs} versus iodoacetamide concentration (Figure 5B) reflects saturation of the enzyme with the inactivator. Equation 6 was used to fit the data and define the values for K_I, 2.5 ± 0.6 mM (concentration of iodoacetamide that

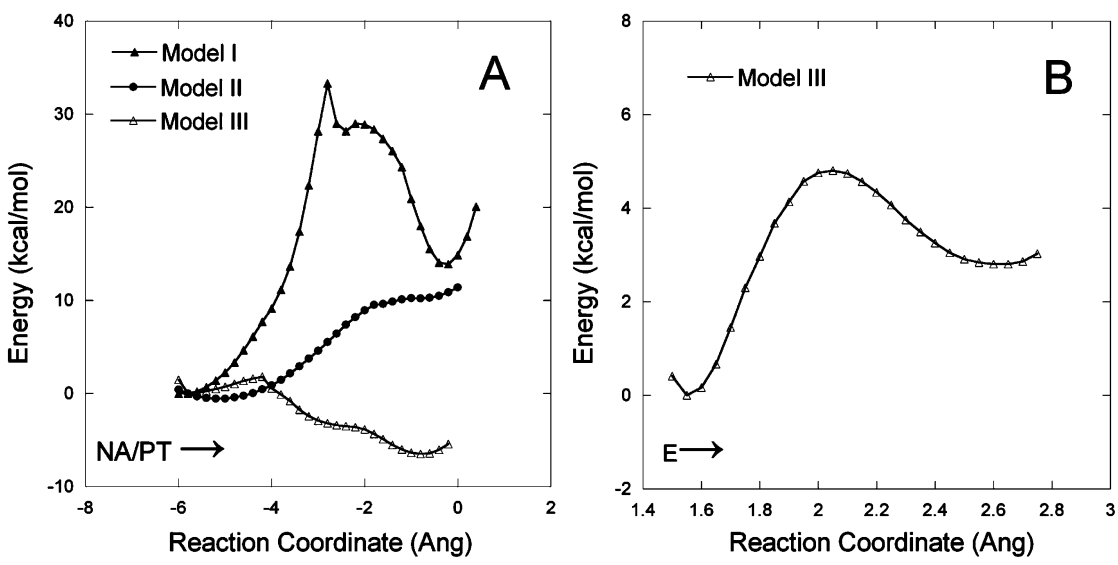

FIGURE 6: (A) Energy profiles for the nucleophilic addition and/or proton transfer in three models. (B) Energy profile for the His-assisted elimination of ammonia from the tetrahedral intermediate of model III.

corresponds to 50% inactivation), and k_{inact}, 0.111 ± 0.008 min^{-1} (the inactivation rate constant).

Next, the pH dependence of the k_{obs} for C265S/C336S BcADI inactivation by 1.5 mM iodoacetamide was measured at 25 °C over the pH range of 5–10 (Figure 5C) which led to determination of a Cys400 thiol pK_a value of 6.9 ± 0.1. This value is ~3 pK_a units lower than the Cys400 thiol pK_a determined for the apoenzyme by UV difference spectroscopy (*vide infra*). For comparison, the pK_a values determined for apo DDAH by carrying out the UV−pH titration, and for DDAH by measuring the pH dependence of the rate constant for iodoacetamide inactivation of DDAH, are equivalent (*62*). These results are consistent with the finding that bound citrulline does not perturb the DDAH Cys thiol pK_a. Taken together, these observations suggest that the Cys thiols of ADI and of DDAH experience different electrostatic environments. The invariant Asp280 of ADI (Figure 2) is replaced by an invariant Lys164 in DDAH. Although the DDAH active site contains a second carboxylate residue (Glu65), its negative charge is neutralized by formation of an ion pair with Lys164. We suspect that the Cys thiol in DDAH is not subjected to the same "negative" electrostatic field that surrounds the Cys thiol in ADI.

QM/MM Analysis of the Impact of the ADI Cys/His Ionization on the Reaction Energy Barrier. Experimental investigations of the ionization of the catalytic Cys thiol in ADI (this work), DDAH (*62*), and PAD4 (*67*) evidenced three unique scenarios. PAD4, which displays an optimal pH range of 7.5–8.5 based on the log(k_{cat}/K_m) versus pH plot and an optimal pH range of 7.2–8.0 based on the log k_{cat} versus pH plot, employs a "reverse protonation mechanism" wherein the pK_a of the active site His imidazolium ion is estimated to be 7.3 and the pK_a of the catalytic Cys thiol is estimated to be 8.3 in the free enzyme and 7.9 in the enzyme–substrate complex. Because the His side chain is not anchored by an active residue (for instance, by the Glu224 in PaADI), it has been argued that the oppositely charged side chains of the catalytic PAD4 His and Cys can assume conformations which bring the point charges sufficiently close for stabilizing electrostatic interaction (*67*). The ADI and DDAH His is anchored by a conserved Glu and is not within interaction range of the Cys. The pK_a of the DDAH Cys is reduced from 8.9 in the free enzyme to ~7.3 in the enzyme–substrate complex (consistent with the pH range of 7−8 for optimal function defined by the log k_{cat} vs pH profile). The substrate-assisted mechanism, wherein the positively charged guanidinium group of the substrate engages in formation of an ion pair with the Cys thiolate anion, has been proposed to account for DDAH catalysis (*62*). In this study, we have shown that the pK_a of catalytic Cys400 in apo BcADI is perturbed upward to 9.6 and downward to 6.9 upon binding a neutral ligand (viz. iodoacetamide).

QM/MM calculations have been performed with PaADI models to explore two possible mechanisms for formation of the His-Cys ion pair upon binding of L-arginine to the ADI active site. The substrate-mediated mechanism (*43*) involves transfer of a proton from the PaADI Cys406 nucleophile to the nearby His278 general acid/base via the L-arginine substrate. Model I, which is used to examine the energy profile associated with the substrate-mediated mechanism, begins with neutral Cys406 and His278 in apo PaADI. The substrate-assisted mechanism (*62*) involves solvent deprotonation of the PaADI Cys406 thiol upon binding of the L-arginine substrate. Two models are examined. Model II begins with the ionized Cys406 side chain (thiolate) and neutral His278 imidazole in the PaADI(L-arginine) complex. Model III begins with the Cys406 thiolate and the His278 imidazolium ion in the PaADI(L-arginine) complex.

The energy profiles calculated for the formation of the tetrahedral intermediate 1 (see Figure 1) are shown in Figure 6A. Snapshots of the stationary points of models I and III are shown in Figure 7, and the key geometric parameters of all stationary points are listed in Table 2.

The substrate-mediated mechanism in which the thiol proton of Cys406 is transferred through the arginine substrate to His278 is examined first. The active site geometry is close to that observed in the earlier MD study (*43*). As shown in Figure 7, the substrate guanidino group is held in place by hydrogen bonds to Asp280 and Asp166 while the nucleo-

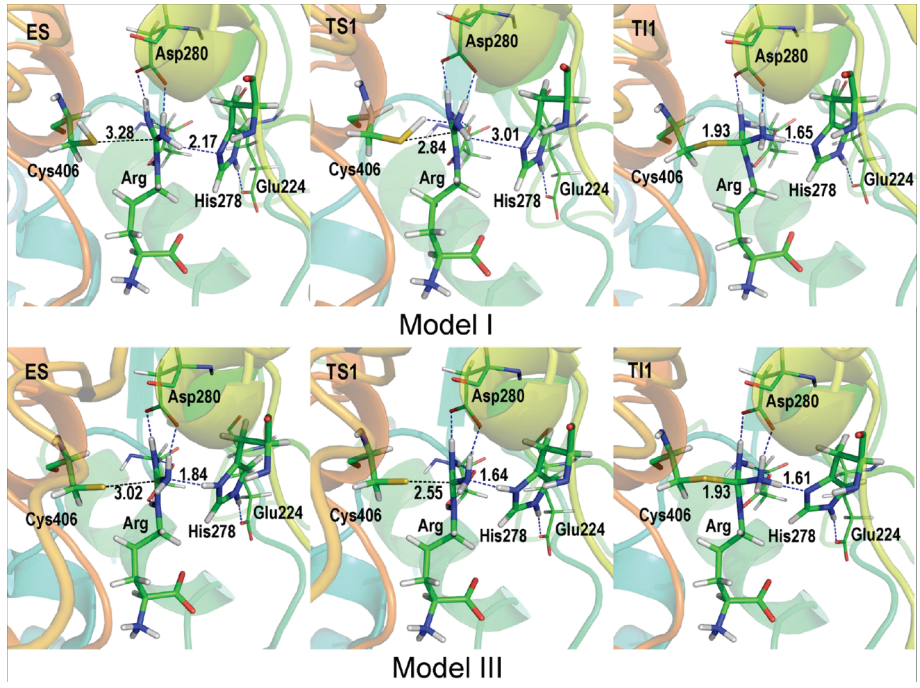

FIGURE 7: Stationary points along the nucleophile addition/proton transfer reaction path for model I and model III. The internuclear distances (dashed lines) are given in angstroms.

Table 2: Key Geometric Parameters of Stationary Points along the Nucleophilic Addition/Proton Transfer Reaction Path

	model I			model II		model III		
distance (Å)	ES	TS1	TI1	ES	TI1[a]	ES	TS1	TI1
S_γ(C406)−C_ζ(Arg)	3.28	2.84	1.93	3.20	2.01	3.02	2.55	1.93
C_ζ(Arg)−$N_{\eta 1}$(Arg)	1.35	1.38	1.58	1.36	1.47	1.38	1.42	1.55
H_γ(C406)−$N_{\eta 1}$(Arg)	4.07	1.57	1.02	–	–	–	–	–
S_γ(C406)−H_γ(C406)	1.35	1.47	2.75	–	–	–	–	–
H_{11}(Arg)−$O_{\delta 1}$(D280)	1.56	1.52	1.52	1.57	1.60	1.60	1.59	1.63
H_{21}(Arg)−$O_{\delta 2}$(D280)	1.62	1.61	1.62	1.61	1.73	1.55	1.58	1.65
H_{22}(Arg)−$O_{\delta 1}$(D166)	1.63	1.59	1.68	1.70	1.79	1.64	1.65	1.69
H_ϵ(Arg)−$O_{\delta 2}$(D166)	1.63	1.62	1.63	1.68	1.76	1.62	1.65	1.63
H_{12}(Arg)−$N_{\delta 1}$(H278)	2.17	3.01	1.65	2.29	2.17	–	–	–
H_δ(H278)−$N_{\eta 1}$(Arg)	–	–	–	–	–	1.84	1.64	1.09
H_δ(H278)−$N_{\delta 1}$(H278)	–	–	–	–	–	1.06	1.08	1.61
$H_{\epsilon 2}$(H278)−$O_{\epsilon 1}$(E224)	1.75	1.77	1.72	1.79	1.81	1.62	1.65	1.71

[a] The tetrahedral intermediate was arbitrarily chosen because no minimum was found.

philic Cys406 and His278 are positioned on the opposite faces of the L-arginine guanidinium carbon. The Cys thiol group is in a near-attack position, in which the distance between S_γ of Cys406 and C_ζ of the substrate is 3.28 Å. The composite reaction coordinate for the nucleophilic addition/proton transfer (NA/PT) step is defined in this model as $\xi = r_1 + r_2 - r_3$, where r_1, r_2, and r_3 are the S_γ−C_ζ, H_γ−$N_{\eta 1}$, and S_γ−H_γ, distances, respectively. The energy profile shown in Figure 6A displays a significant energy barrier of ~33 kcal/mol to the tetrahedral intermediate. (The sharp peak near $\xi = -2.8$ corresponds to a conformational change in the Cys thiol as it approaches the substrate.) As shown in Figure 7 and Table 2, the transition-state structure suggests that the transfer of a proton from the Cys406 thiol to the L-arginine guanidino nitrogen atom occurs in concert with nucleophilic addition. At the tetrahedral intermediate, the proton is bonded to $N_{\eta 1}$ of the substrate, and a hydrogen bond has been formed between H_{12} and N_δ of His278. The NH_3 leaving group is ideally positioned for the elimination. As shown in Figure 7, the C_ζ atom in the tetrahedral intermediate is sp^3 hybridized. The high barrier associated with the substrate-assisted pathway is consistent with earlier DFT results based on truncated active-site models (*43*).

In model II, the reaction coordinate is defined as the distance between S_γ and C_ζ: $\xi = r_1$. Despite the absence of the Cys406 thiol proton, the PaADI(L-arginine) complex (not shown here) is quite similar to that observed with model I, with a slightly shorter S_γ−C_ζ distance (3.20 Å). The energy profile calculated for model II, and shown in Figure 6A, contains a comparatively smaller energy barrier, yet the tetrahedral intermediate formed is not stabilized as is evidenced by the absence of an "energy well". Moreover, we know that this intermediate state cannot eliminate ammonia which is needed to partition forward. Thus, we proceed to model III.

As shown in Figure 7, the His278 imidazolium ion proton of the PaADI(L-arginine) complex, assumed in model III, engages in a hydrogen bond with $N_{\eta 1}$ of L-arginine. The position of the Cys406 sulfur atom is unchanged except for a shorter S_γ−C_ζ distance of 3.02 Å. We found that it is convenient to define the reaction coordinate as follows: $\xi = r_1' + r_2' - r_3'$, where r_1', r_2', and r_3' are the S_γ−C_ζ, H_δ−$N_{\eta 1}$,

and $N_\delta - H_\delta$ distances, respectively. The asymmetric proton transfer coordinate is included to render a smooth reaction path. The model III energy profile (Figure 6A) indicates that the nucleophilic addition of the thiolate to the guanidino C_ζ atom does not encounter a high-energy barrier. Specifically, the height of the energy barrier near $\xi = 4.2$ is approximately 2.0 kcal/mol, consistent with the strong nucleophilicity of the thiolate anion. As depicted in Figure 7 and as reported in Table 2, the tetrahedral intermediate is quite similar to that of model I. In particular, the "NH_3" group is hydrogen bonded with His278, ready for elimination. Also, we report in Table 2 that in all three models the hydrogen bonds with Asp280 and Asp166 and that between His278 and Glu224 are maintained throughout the reaction.

We have further examined the elimination step from the tetrahedral intermediate using model III. The energy profile shown in Figure 6B indicates that the elimination of the ammonia leaving group proceeds through a very low barrier. Although the energy barriers in the reaction path calculations do not include the entropic contributions, they do nonetheless indicate a preferred pathway as dictated by the electrostatic forces. On the basis of the results obtained from this computational analysis, we conclude that the catalytically active configuration of the active site in the ADI(L-arginine) complex consists of the Cys thiolate anion and His imidazolium cation.

CONCLUSION

The three members of the GMSF (ADI, DDAH, and PAD4) share the common feature of nucleophilic catalysis by a Cys thiolate and general acid catalysis by a His imidazolium ion. All three enzymes rely on electrostatic effects to reduce the pK_a of the Cys thiol so that the Cys thiol is ionized at the optimal pH range. For PAD4 and DDAH, this pH range is 7−8, whereas for ADI, it extends to pH 5. Thus, ADI must employ comparatively stronger electrostatic forces to achieve a greater reduction in the Cys thiol pK_a. The observation that the Cys thiol in the apoenzyme has a pK_a of 9.6 showed that the substrate ligand is required to stabilize the Cys thiolate. The ionization of the Cys nucleophile is most likely due to the exertion of the positive electrostatic field from the L-arginine guanidinium group. The guanidinium group both shields the Cys thiol from the negative electrostatic field that emanates from the two neighboring Asp carboxylate groups and provides a point charge for favorable electrostatic interaction with the charged Cys sulfur atom. The proton that dissociates from the Cys thiol is presumably captured by a solvent water molecule.

SUPPORTING INFORMATION AVAILABLE

A figure showing the SDS−PAGE gel of purified BcADI, EcADI, and BmADI and a figure reporting the covalent adducts formed in the iodoacetamide inactivation of BcADI. This material is available free of charge via the Internet at http://pubs.acs.org.

REFERENCES

1. Schimke, R. T., Berlin, C. M., Sweeney, E. W., and Carroll, W. R. (1966) The generation of energy by the arginine dihydrolase pathway in *Mycoplasma hominis* 07. *J. Biol. Chem. 241*, 2228–2236.
2. Smith, D. W., Ganaway, R. L., and Fahrney, D. E. (1978) Arginine deiminase from *Mycoplasma arthritidis*. Structure-activity relationships among substrates and competitive inhibitors. *J. Biol. Chem. 253*, 6016–6020.
3. Cunin, R., Glansdorff, N., Pierard, A., and Stalon, V. (1986) Biosynthesis and metabolism of arginine in bacteria. *Microbiol. Rev. 50*, 314–352.
4. Zuniga, M., Perez, G., and Gonzalez-Candelas, F. (2002) Evolution of arginine deiminase (ADI) pathway genes. *Mol. Phylogenet. Evol. 25*, 429–444.
5. Dong, Y., Chen, Y. Y., Snyder, J. A., and Burne, R. A. (2002) Isolation and molecular analysis of the gene cluster for the arginine deiminase system from *Streptococcus gordonii* DL1. *Appl. Environ. Microbiol. 68*, 5549–5553.
6. Gruening, P., Fulde, M., Valentin-Weigand, P., and Goethe, R. (2006) Structure, regulation, and putative function of the arginine deiminase system of *Streptococcus suis*. *J. Bacteriol. 188*, 361–369.
7. Makhlin, J., Kofman, T., Borovok, I., Kohler, C., Engelmann, S., Cohen, G., and Aharonowitz, Y. (2007) *Staphylococcus aureus* ArcR controls expression of the arginine deiminase operon. *J. Bacteriol. 189*, 5976–5986.
8. Seggewiss, J., Becker, K., Kotte, O., Eisenacher, M., Yazdi, M. R., Fischer, A., McNamara, P., Al Laham, N., Proctor, R., Peters, G., Heinemann, M., and von Eiff, C. (2006) Reporter metabolite analysis of transcriptional profiles of a *Staphylococcus aureus* strain with normal phenotype and its isogenic hemB mutant displaying the small-colony-variant phenotype. *J. Bacteriol. 188*, 7765–7777.
9. Silva, L. M., Baums, C. G., Rehm, T., Wisselink, H. J., Goethe, R., and Valentin-Weigand, P. (2006) Virulence-associated gene profiling of *Streptococcus suis* isolates by PCR. *Vet. Microbiol. 115*, 117–127.
10. Knodler, L. A., Sekyere, E. O., Stewart, T. S., Schofield, P. J., and Edwards, M. R. (1998) Cloning and expression of a prokaryotic enzyme, arginine deiminase, from a primitive eukaryote *Giardia intestinalis*. *J. Biol. Chem. 273*, 4470–4477.
11. Adam, R. D. (2001) Biology of *Giardia lamblia*. *Clin. Microbiol. Rev. 14*, 447–475.
12. Morrison, H. G., McArthur, A. G., Gillin, F. D., Aley, S. B., Adam, R. D., Olsen, G. J., Best, A. A., Cande, W. Z., Chen, F., Cipriano, M. J., Davids, B. J., Dawson, S. C., Elmendorf, H. G., Hehl, A. B., Holder, M. E., Huse, S. M., Kim, U. U., Lasek-Nesselquist, E., Manning, G., Nigam, A., Nixon, J. E., Palm, D., Passamaneck, N. E., Prabhu, A., Reich, C. I., Reiner, D. S., Samuelson, J., Svard, S. G., and Sogin, M. L. (2007) Genomic minimalism in the early diverging intestinal parasite *Giardia lamblia*. *Science 317*, 1921–1926.
13. Noh, E. J., Kang, S. W., Shin, Y. J., Kim, D. C., Park, I. S., Kim, M. Y., Chun, B. G., and Min, B. H. (2002) Characterization of mycoplasma arginine deiminase expressed in *E. coli* and its inhibitory regulation of nitric oxide synthesis. *Mol. Cells 13*, 137–143.
14. Palm, J. E., Weiland, M. E., Griffiths, W. J., Ljungstrom, I., and Svard, S. G. (2003) Identification of immunoreactive proteins during acute human giardiasis. *J. Infect. Dis. 187*, 1849–1859.
15. Shirai, H., Blundell, T. L., and Mizuguchi, K. (2001) A novel superfamily of enzymes that catalyze the modification of guanidino groups. *Trends Biochem. Sci. 26*, 465–468.
16. Leiper, J. M., Santa Maria, J., Chubb, A., MacAllister, R. J., Charles, I. G., Whitley, G. S., and Vallance, P. (1999) Identification of two human dimethylarginine dimethylaminohydrolases with distinct tissue distributions and homology with microbial arginine deiminases. *Biochem. J. 343*, 209–214.
17. Santa Maria, J., Vallance, P., Charles, I. G., and Leiper, J. M. (1999) Identification of microbial dimethylarginine dimethylaminohydrolase enzymes. *Mol. Microbiol. 33*, 1278–1289.
18. Kearney, P. L., Bhatia, M., Jones, N. G., Yuan, L., Glascock, M. C., Catchings, K. L., Yamada, M., and Thompson, P. R. (2005) Kinetic characterization of protein arginine deiminase 4: A transcriptional corepressor implicated in the onset and progression of rheumatoid arthritis. *Biochemistry 44*, 10570–10582.
19. Nakada, Y., and Itoh, Y. (2003) Identification of the putrescine biosynthetic genes in *Pseudomonas aeruginosa* and characterization of agmatine deiminase and N-carbamoylputrescine amidohydrolase of the arginine decarboxylase pathway. *Microbiology 149*, 707–714.
20. Tocilj, A., Schrag, J. D., Li, Y., Schneider, B. L., Reitzer, L., Matte, A., and Cygler, M. (2005) Crystal structure of N-succinylarginine dihydrolase AstB, bound to substrate and product, an enzyme from

the arginine catabolic pathway of *Escherichia coli*. *J. Biol. Chem. 280*, 15800–15808.
21. Vallance, P., and Leiper, J. (2002) Blocking NO synthesis: How, where and why? *Nat. Rev. Drug Discovery 1*, 939–950.
22. Thompson, P. R., and Fast, W. (2006) Histone citrullination by protein arginine deiminase: Is arginine methylation a green light or a roadblock? *ACS Chem. Biol. 1*, 433–441.
23. Wang, Y., Wysocka, J., Sayegh, J., Lee, Y. H., Perlin, J. R., Leonelli, L., Sonbuchner, L. S., McDonald, C. H., Cook, R. G., Dou, Y., Roeder, R. G., Clarke, S., Stallcup, M. R., Allis, C. D., and Coonrod, S. A. (2004) Human PAD4 regulates histone arginine methylation levels via demethylimination. *Science 306*, 279–283.
24. Schellekens, G. A., de Jong, B. A., van den Hoogen, F. H., van de Putte, L. B., and van Venrooij, W. J. (1998) Citrulline is an essential constituent of antigenic determinants recognized by rheumatoid arthritis-specific autoantibodies. *J. Clin. Invest. 101*, 273–281.
25. Arita, K., Hashimoto, H., Shimizu, T., Nakashima, K., Yamada, M., and Sato, M. (2004) Structural basis for Ca^{2+}-induced activation of human PAD4. *Nat. Struct. Mol. Biol. 11*, 777–783.
26. Das, K., Butler, G. H., Kwiatkowski, V., Clark, A. D., Jr., Yadav, P., and Arnold, E. (2004) Crystal structures of arginine deiminase with covalent reaction intermediates: Implications for catalytic mechanism. *Structure 12*, 657–667.
27. Fritsche, E., Bergner, A., Humm, A., Piepersberg, W., and Huber, R. (1998) Crystal structure of L-arginine:inosamine-phosphate amidinotransferase StrB1 from *Streptomyces griseus*: An enzyme involved in streptomycin biosynthesis. *Biochemistry 37*, 17664–17672.
28. Fritsche, E., Humm, A., and Huber, R. (1999) The ligand-induced structural changes of human L-arginine:glycine amidinotransferase. A mutational and crystallographic study. *J. Biol. Chem. 274*, 3026–3032.
29. Galkin, A., Kulakova, L., Sarikaya, E., Lim, K., Howard, A., and Herzberg, O. (2004) Structural insight into arginine degradation by arginine deiminase, an antibacterial and parasite drug target. *J. Biol. Chem. 279*, 14001–14008.
30. Galkin, A., Lu, X., Dunaway-Mariano, D., and Herzberg, O. (2005) Crystal structures representing the Michaelis complex and the thiouronium reaction intermediate of *Pseudomonas aeruginosa* arginine deiminase. *J. Biol. Chem. 280*, 34080–34087.
31. Humm, A., Fritsche, E., and Steinbacher, S. (1997) Structure and reaction mechanism of L-arginine:glycine amidinotransferase. *Biol. Chem. 378*, 193–197.
32. Llacer, J. L., Polo, L. M., Tavarez, S., Alarcon, B., Hilario, R., and Rubio, V. (2007) The gene cluster for agmatine catabolism of *Enterococcus faecalis*: Study of recombinant putrescine transcarbamylase and agmatine deiminase and a snapshot of agmatine deiminase catalyzing its reaction. *J. Bacteriol. 189*, 1254–1265.
33. Luo, Y., Arita, K., Bhatia, M., Knuckley, B., Lee, Y. H., Stallcup, M. R., Sato, M., and Thompson, P. R. (2006) Inhibitors and inactivators of protein arginine deiminase 4: Functional and structural characterization. *Biochemistry 45*, 11727–11736.
34. Murray-Rust, J., Leiper, J., McAlister, M., Phelan, J., Tilley, S., Santa Maria, J., Vallance, P., and McDonald, N. (2001) Structural insights into the hydrolysis of cellular nitric oxide synthase inhibitors by dimethylarginine dimethylaminohydrolase. *Nat. Struct. Biol. 8*, 679–683.
35. Lu, X., Galkin, A., Herzberg, O., and Dunaway-Mariano, D. (2004) Arginine deiminase uses an active-site cysteine in nucleophilic catalysis of L-arginine hydrolysis. *J. Am. Chem. Soc. 126*, 5374–5375.
36. Stone, E. M., Person, M. D., Costello, N. J., and Fast, W. (2005) Characterization of a transient covalent adduct formed during dimethylarginine dimethylaminohydrolase catalysis. *Biochemistry 44*, 7069–7078.
37. Lu, X., Li, L., Wu, R., Feng, X., Li, Z., Yang, H., Wang, C., Guo, H., Galkin, A., Herzberg, O., Mariano, P. S., Martin, B. M., and Dunaway-Mariano, D. (2006) Kinetic analysis of *Pseudomonas aeruginosa* arginine deiminase mutants and alternate substrates provides insight into structural determinants of function. *Biochemistry 45*, 1162–1172.
38. Hong, L., and Fast, W. (2007) Inhibition of human dimethylarginine dimethylamionhydrolase-1 by S-nitroso-L-homocysteine and hydrogen peroxide: Analysis, quantification, and implications for hyperhomocysteinemia. *J. Biol. Chem. 282*, 34684–34692.
39. Lu, X., Li, L., Feng, X., Wu, Y., Dunaway-Mariano, D., Engen, J. R., and Mariano, P. S. (2005) L-Canavanine is a time-controlled mechanism-based inhibitor of *Pseudomonas aeruginosa* arginine deiminase. *J. Am. Chem. Soc. 127*, 16412–16413.
40. Luo, Y., Knuckley, B., Lee, Y. H., Stallcup, M. R., and Thompson, P. R. (2006) A fluoroacetamidine-based inactivator of protein arginine deiminase 4: Design, synthesis, and in vitro and in vivo evaluation. *J. Am. Chem. Soc. 128*, 1092–1093.
41. Stone, E. M., Schaller, T. H., Bianchi, H., Person, M. D., and Fast, W. (2005) Inactivation of two diverse enzymes in the amidinotransferase superfamily by 2-chloroacetamidine: Dimethylarginine and peptidylarginine deiminase. *Biochemistry 44*, 13744–13752.
42. Wei, Y., Zhou, H., Sun, Y., He, Y., and Luo, Y. (2007) Insight into the catalytic mechanism of arginine deiminase: Functional studies on the crucial sites. *Proteins 66*, 740–750.
43. Wang, C., Xu, D., Zhang, L., Xie, D., and Guo, H. (2007) Molecular dynamics and density functional studies of substrate binding and catalysis of arginine deiminase. *J. Phys. Chem. B 111*, 3267–3273.
44. Li, L., Li, Z., Chen, D., Lu, X., Wright, E. C., Solberg, N. O., Green-Church, K. B., Zhang, L., Galkin, A., Kulakova, L., Herzberg, O., Dunaway-Mariano, D., and Mariano, P. S. (2008) Inactivation of microbial arginine deiminases by L-canavanine. *J. Am. Chem. Soc. 130*, 1918–1931.
45. Prescott, L. M., and Jones, M. E. (1969) Modified methods for the determination of carbamyl aspartate. *Anal. Biochem. 32*, 408–419.
46. Weickmann, J. L., and Fahrney, D. E. (1977) Arginine deiminase from *Mycoplasma arthritidis*. Evidence for multiple forms. *J. Biol. Chem. 252*, 2615–2620.
47. Brooks, B. R., Bruccoleri, R. E., Olafson, B. D., States, D. J., Swaminathan, S., and Karplus, M. (1983) CHARMM: A program for macromolecular energy, minimization, and dynamics calculations. *J. Comput. Chem. 4*, 187–217.
48. Brooks, C. L., Brunger, A., and Karplus, M. (1985) Active site dynamics in protein molecules: A stochastic boundary molecular-dynamics approach. *Biopolymers 24*, 843–865.
49. Warshal, A., and Levitt, M. (1976) Theoretical studies of enzymatic reactions: Dielectric, electrostation and steric stabilization of carbonium ion in the reaction of lysozyme. *J. Mol. Biol. 103*, 227–249.
50. Gao, J. (1996) Methods and applications of combined quantum mechanical and molecular mechanical potentials, in *Reviews in Computational Chemistry* (Lipkowitz, K. B., and Boyd, D. B., Eds.) pp 119–185, VCH, New York.
51. Lopez, X., and York, D. M. (2003) Parameterization of semiempirical methods to treat nucleophilic attacks to biological phosphates: AM1/d parameters for phosphorus. *Theor. Chem. Acc. 109*, 149–159.
52. Becke, A. D. (1993) Density-functional thermochemistry. III. The role of exact exchange. *J. Chem. Phys. 98*, 5648–5652.
53. Lee, C., Yang, W., and Parr, R. G. (1988) Development of the Colle-Salvetti correlation-energy formula into a functional of the electron density. *Phys. Rev. B 37*, 785–789.
54. MacKerell, A. D., Jr., Bashford, D., Bellott, D., Dunbrack, R. L., Jr., Evanseck, J. D., Field, M. J., Fischer, S., Gao, J., Guo, H., Ha, S., Joseph-McCarthy, D., Kuchnir, L., Kuczera, K., Lau, F. T. K., Mattos, C., Michnick, S., Ngo, T., Nguyen, D. T., Prodhom, B., Reiher, W. E., III, Roux, B., Schlenkrich, M., Smith, J. C., Stote, R., Straub, J., Watanabe, M., Wiórkiewicz-Kuczera, J., Yin, D., and Karplus, M. (1998) All-atom empirical potential for molecular modeling and dynamics studies of proteins. *J. Phys. Chem. B 102*, 3586–3616.
55. Field, M. J., Bash, P. A., and Karplus, M. (1990) A combined quantum mechanical and molecular mechanical potential for molecular dynamics simulations. *J. Comput. Chem. 11*, 700–733.
56. Eurenius, K. P., Chatfield, D. C., Brooks, B. R., and Hodoscek, M. (1996) Enzyme mechanisms with hybrid quantum and molecular mechanical potentials. I. Theoretical considerations. *Int. J. Quantum Chem. 60*, 1189–1200.
57. Polgar, L. (1974) Spectrophotometric determination of mercaptide ion, an activated form of SH-group in thiol enzymens. *FEBS Lett. 38*, 187–190.
58. Graminski, G. F., Kubo, Y., and Armstrong, R. N. (1989) Spectroscopic and kinetic evidence for the thiolate anion of glutathione at the active site of glutathione S-transferase. *Biochemistry 28*, 3562–3568.
59. Lo Bello, M., Parker, M. W., Desideri, A., Polticelli, F., Falconi, M., Del Boccio, G., Pennelli, A., Federici, G., and Ricci, G. (1993) Peculiar spectroscopic and kinetic properties of Cys-47 in human placental glutathione transferase: Evidence for an atypical thiolate ion pair near the active site. *J. Biol. Chem. 268*, 19033–19038.

60. Nelson, J. W., and Creighton, T. E. (1994) Reactivity and ionization of the active site cysteine residues of DsbA, a protein required for disulfide bond formation in vivo. *Biochemistry 33*, 5974–5983.
61. Sarkany, Z., Szeltner, Z., and Polgar, L. (2001) Thiolate-imidazolium ion pair is not an obligatory catalytic entity of cysteine peptidases: The active site of picornain 3C. *Biochemistry 40*, 10601–10606.
62. Stone, E. M., Costello, A. L., Tierney, D. L., and Fast, W. (2006) Substrate-assisted cysteine deprotonation in the mechanism of dimethylargininase (DDAH) from *Pseudomonas aeruginosa*. *Biochemistry 45*, 5618–5630.
63. Wang, P. F., McLeish, M. J., Kneen, M. M., Lee, G., and Kenyon, G. L. (2001) An unusually low pK_a for Cys282 in the active site of human muscle creatine kinase. *Biochemistry 40*, 11698–11705.
64. Dyson, H. J., Jeng, M. F., Tennant, L. L., Slaby, I., Lindell, M., Cui, D. S., Kuprin, S., and Holmgren, A. (1997) Effects of buried charged groups on cysteine thiol ionization and reactivity in *Escherichia coli* thioredoxin: Structural and functional characterization of mutants of Asp 26 and Lys 57. *Biochemistry 36*, 2622–2636.
65. Tolbert, B. S., Tajc, S. G., Webb, H., Snyder, J., Nielsen, J. E., Miller, B. L., and Basavappa, R. (2005) The active site cysteine of ubiquitin-conjugating enzymes has a significantly elevated pK_a: Functional implications. *Biochemistry 44*, 16385–16391.
66. Krekel, F., Samland, A. K., Macheroux, P., Amrhein, N., and Evans, J. N. (2000) Determination of the pKa value of C115 in MurA (UDP-N-acetylglucosamine enolpyruvyltransferase) from *Enterobacter cloacae*. *Biochemistry 39*, 12671–12677.
67. Knuckley, B., Bhatia, M., and Thompson, P. R. (2007) Protein arginine deiminase 4: Evidence for a reverse protonation mechanism. *Biochemistry 46*, 6578–6587.

BI7023496